INSTITUTE OF PHYSICS PUBLISHING JOURNAL OF PHYSICS D: APPLIED PHYSICS

J. Phys. D: Appl. Phys. **39** (2006) 1312–1325 doi:10.1088/0022-3727/39/7/S05

Dielectric relaxation in composites containing electrically isolated particles with thin semi-continuous metal coatings

I J Youngs[1,4], **N Bowler**[2] **and O Ugurlu**[3]

[1] Physical Sciences Department, Dstl, Porton Down, Salisbury, Wiltshire, SP4 0JQ, UK
[2] Center for NDE, Iowa State University, 279 ASC II, 1915 Scholl Road, Ames, IA 50011-3042, USA
[3] Department of Materials Science and Engineering, Iowa State University, IA, USA

E-mail: ijyoungs@dstl.gov.uk

Received 26 October 2005
Published 17 March 2006
Online at stacks.iop.org/JPhysD/39/1312

Abstract

The dielectric relaxation due to interfacial charges in metal particle-filled composites occurs in the optical (high frequency) regime. However, many applications would benefit from a shift of the relaxation to a much lower frequency regime (e.g. radio or microwave range). This could be achieved by using a filler with reduced conductivity, but there is no continuum of conductivity in naturally occurring materials to allow engineers to readily achieve this aim or to have complete design freedom. Recently, it was demonstrated, experimentally and theoretically, how insulating particles with nano-scale metal coatings enable this relaxation to be shifted to a lower frequency regime. The current work investigates the microstructure of the metal coating, highlighting a semi-continuous coating structure. Therefore, the relevance of a two-dimensional (2D) percolation-based model to describe the effective dielectric properties of the coating is explored. It is demonstrated that a model in which the metal coating is assumed to be near the 2D percolation threshold can provide a reasonable fit to the experimental data. An improved fit is achieved when a distribution of metal area coverage is permitted.

(Some figures in this article are in colour only in the electronic version)

1. Introduction

Engineering the electromagnetic properties of materials is of significant technological interest, especially at microwave (and perhaps now more broadly from radio to millimetre wavelengths) and optical frequencies for communications applications. However, component and system design is hampered by a limited design space for the relevant material properties and a design space that is, in many cases, only sparsely and discretely filled by available materials. It is clear that engineers would prefer a design space that bounds a continuum of options to realize optimum designs with improved trade-offs with other design parameters. Recently there has been growing interest in the use of metal coated nano-particles to engineer optical dielectric response for applications including filters and polarizers and to achieve enhanced non-linear effects [1–4]. In contrast, the use of metal-coated particles at microwave frequencies has been recommended more from a desire to develop lightweight equivalents to composites containing solid filler particles rather than as a mechanism to provide greater design freedom [5–8]. The authors have recently presented experimental evidence confirming the potential for engineering metal-coated particles to achieve microwave dielectric loss via a mechanism analogous to the aforementioned optical response of coated nano-particles [9]; noting that the study was underpinned by previously developed particle engineering methods and extrinsic evidence of microwave absorption

[4] Author to whom any correspondence should be addressed. Rm14, Bldg 352, Dstl, Porton Down, Salisbury, Wiltshire, SP4 0JQ, UK.

through reflectivity calculations [10]. The critical feature of the coated particles studied herein and in [9] is the presence of an insulating outer layer. This layer minimizes, and ideally eliminates, conduction losses especially at high filler concentrations that would normally be derived from conduction through connected particle networks within the composite in the absence of such an insulating outer coating. Hence, the dielectric loss process can be studied in isolation, enabling investigation of appropriate theoretical models for the dielectric response to facilitate efficient design.

As background to the current study it is appropriate to review the initial model developed in [9]. In support of the initial model little was known about the physical nature of the metal coating, and it was assumed that the coating was uniform and continuous on each particle. For reference the geometry and composition of the particles studied is summarized in figure 1(*a*) and table 1. The theoretical calculation of the permittivity of the composite initially used the Rayleigh (or Maxwell–Garnett) effective medium model extended to the case of a 4-layered, spherical filler particle following the approach of Sihvola and Lindell [18] but demonstrated the validity of a 2-layer approximation using an effective medium approximation for the hollow core particle ($\varepsilon_{\text{core}} = 1.72 - j\,(8.3 \times 10^{-3})$ and $a_{\text{core}} = 15\,\mu$m), retaining the metal coating layer and assuming that the outermost dielectric coating is insignificant except in influencing the choice of a non-percolative effective medium model in the first instance. This simplification, shown schematically in figure 1(*b*), eased the introduction of a distribution of coating thickness. Equation (1) reproduces the 2-layer particle model employed in [9][5]:

$$\varepsilon = \varepsilon_{\text{m}} + 3\varepsilon_{\text{m}}\frac{S}{1-S},$$

$$S = \frac{4\pi}{3V}\int_0^\infty p(t)(a_2+t)^3 \times \frac{(\varepsilon_1-\varepsilon_{\text{m}})(\varepsilon_2+2\varepsilon_1)(a_2+t)^3+(2\varepsilon_1+\varepsilon_{\text{m}})(\varepsilon_2-\varepsilon_1)a_2^3}{(\varepsilon_1+2\varepsilon_{\text{m}})(\varepsilon_2+2\varepsilon_1)(a_2+t)^3+2(\varepsilon_1-\varepsilon_{\text{m}})(\varepsilon_2-\varepsilon_1)a_2^3}\,\mathrm{d}t, \tag{1}$$

where ε, ε_{m}, ε_1 and ε_2 are the complex relative permittivities of the composite, host medium, filler particle coating and filler particle core, respectively; a_2 is the core radius and t is the coating thickness; and $p(t)$ is the probability of a coating having thickness t. Assuming a normal (or Gaussian) distribution of t leads to the following expression for $p(t)$:

$$p(t) = \frac{1}{\sigma\sqrt{2\pi}}\exp\left(-\frac{1}{2}\left(\frac{t-\bar{t}}{\sigma}\right)^2\right), \tag{2}$$

where $\bar{t}$ is the mean value of t, and σ is the standard deviation. A normal distribution of t gives rise to a finite probability of a coating thickness less than zero, which cannot be permitted physically. Cutting off the normal distribution at $t = 0$, as in equation (1), implies that

$$\int_0^\infty p(t)\mathrm{d}t < 1. \tag{3}$$

[5] It should be noted that the previous work investigated the role of a distribution of particle size (for fixed coating thickness to particle radius ratio) through the application of the Hanai–Bruggeman model extended to the multi-layer filler particle case. It was concluded that a distribution of particle size was not a significant contributor to the broad dielectric relaxation observed experimentally.

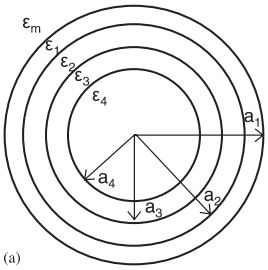

Medium	Material
m	paraffin wax
1	alumina
2	tungsten
3	glass
4	air

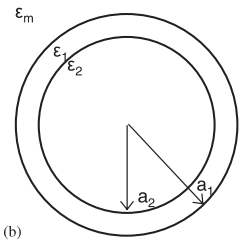

Medium	Material
m	paraffin wax
1	tungsten
2	glass/air effective medium

Figure 1. Filler particle geometry (*a*) full 4-layer particle and (*b*) pseudo 2-layer particle.

Explicit normalization of S, to account for the fact that the integral over the probability distribution is less than unity, is not necessary, however, since the expression for V in terms of $p(t)$ is also cut off at $t = 0$:

$$V = \frac{4\pi}{3\,v_{\text{f}}}\int_0^\infty p(t)(a_2+t)^3\,\mathrm{d}t. \tag{4}$$

The coating permittivity is defined by equation (5) following the low frequency approximation of the Drude model in which σ_1 is the coating conductivity, ω is the angular frequency and ε_0 is the permittivity of free space:

$$\varepsilon_1 = 1 - j\frac{\sigma_1}{\omega\varepsilon_0}. \tag{5}$$

Whilst the inclusion of a distribution of coating thickness enabled an improved fit to the experimental data to be obtained (using the coating conductivity and standard deviation of the coating thickness as fitting parameters), comparison of the fit to the experimental data demonstrated that an additional broadening mechanism was required. The primary role of the coating conductivity is to fit the relaxation frequency, demonstrating that a conductivity well below that of the bulk metal is required. Thus, a second broadening mechanism was introduced by accounting for the nano-scale nature of the metal coating, which also removed the reliance of the model on fitting the coating conductivity. Under these circumstances, equation (5) is replaced by the full Drude model, extended to account for surface scattering of the conduction electrons in the coating, as given by equations (6) and (7). This alternative model includes the coating thickness and hence provides added influence for a distribution of this parameter. It is noted that the inclusion of interband transition terms in equation (6) is assumed to be unnecessary because the current work is focused on response in a much lower frequency range.

$$\varepsilon_1 = 1 - \frac{\omega_{\text{p}}^2}{\omega(\omega - j/\tau)}, \tag{6}$$

$$\frac{1}{\tau} = \frac{1}{\tau_{\text{bulk}}} + A\frac{v_{\text{F}}}{l_{\text{path}}}. \tag{7}$$

Table 1. Physical properties of coated particles.

Parameter	Value	Source/comment
Coated particle		
Density (g cm^{-3})	0.62	[11], value used in formulating composites
	0.539 ± 0.026	Measured by Helium pycnometer
Crush pressure (MPa)	69	[10]
Core particle	Glass microbubble	3M™Scotchlite™ S60
Density (g cm^{-3})	0.60	[12]
Mean radius (μm)	15	[12]
10th centile radius (μm)	7.5	[12]
90th centile radius (μm)	27.5	[12]
Shell material	Soda-lime-borosilicate glass	[12]
Shell density (g cm^{-3})	2.5	[13], estimated from values for A and E glass
Shell thickness (μm)	1.311	Calculated from particle and shell densities for mean particle size
Shell real permittivity	4.8	[14], pyrex, 25 °C, 10 GHz
Shell loss tangent ($\times 10^4$)	98	[14], pyrex, 25 °C, 10 GHz
Core material	Air	Assumed
Tungsten coating		
Thickness (nm)	20	[11], mean value
Bulk conductivity (Sm^{-1})	1.77e7	[15]
Bulk plasma frequency ω_p (eV)	7.6	[16], theoretical
Bulk relaxation time τ_{bulk} (s)	$173.133/\omega_p$	Calculated from bulk conductivity
Bulk Fermi velocity v_F (ms^{-1})	9.6e5	[17], theoretical
Alumina outer coating		
Thickness (nm)	3	[11]
Real permittivity	8.79	[14], Coors, 25 °C, 10 GHz
Loss tangent ($\times 10^4$)	18	[14], Coors, 25 °C, 10 GHz

The parameters in equations (6) and (7) are defined as follows: ω_p is the plasma frequency, τ is the electronic relaxation time, τ_{bulk} is the relaxation time for the bulk metal, A is a parameter that is reported to represent the degree to which the local chemical environment influences scattering of the conduction electrons in the metal film, and it is taken to lie in the range 0.25–2 [4, 19], v_F is the Fermi velocity and l_{path} is the mean free path.

For solid nano-particles the mean free path is generally taken to be the particle radius, but for metallic shells the following expression has been proposed [20]. Using the notation for our 2-layer particles, the expression,

$$l_{path} = \sqrt[3]{(a_1 - a_2)(a_1^2 - a_2^2)}, \tag{8}$$

yields a value of $l_{path} = 229$ nm in this case. If it is assumed that the mean free path is constrained between this value and the coating thickness, then the effective relaxation time lies in the range $0.58 \leqslant \tau/\tau_{bulk} \leqslant 0.94$, assuming $A = 1$. The use of these coating thickness related broadening mechanisms is also supported by recent work by Westcott *et al* on the optical absorption line widths of metal coated nano-particles [4].

The previous work demonstrated that, by taking the best case value for the mean free path ($l_{path} = t$, the coating thickness), and representing the permittivity of tungsten in equation (1) by equations (6)–(8), a reasonable fit to experimental data could be obtained for filler concentrations in the range 15–50 vol%. Figure 2 reproduces this comparison from [9], requiring that the mean coating thickness was reduced to 10 nm with a standard deviation of 13 nm and that the parameter A was permitted to vary freely[6]. A value of $A = 4500$ was required to achieve this fit, with the critical observation that such a value is orders of magnitude greater than reported elsewhere in the literature [4, 19, 21, 22]. Nevertheless, such a value is potentially justified by noting that it simply reflects the presence of much stronger free electron scattering than expected, and this was considered plausible since very little was actually known at that time about the true quality of the nano-scale coating. However, it is this knowledge gap and the extreme value for the parameter A that stimulated the further work reported here regarding analysis of the coating and the further development of the model for the permittivity of the metal layer. Indeed, it may be the case

[6] Since the parameter A is used as a fitting parameter, it is relevant to summarize the range of values obtained by previous researchers. Hovel *et al* provide a valuable review of both experimental results and theoretical models for bounding and determining the value of this parameter [19]. Although, it should be noted that most work has been undertaken with respect to analysing Mie resonances from metal nano-particles and nano-particle clusters in the optical regime where A is used to account for damping effects and variations in bandwidth of the absorption bands. It is apparent that the theoretical models do not account for the range of experimental results, especially values below 0.7 and greater than 1 (although, and perhaps crucially here, in terms of classical theory the presence of internal grain boundaries would result in $A > 1$). Hence, it has been postulated that the value of A is typically dominated by chemical interactions at the metal interface and that A increases with the level of interaction. For clusters of silver nano-particles in a range of inert matrices, A is found to lie in the range 0.25–1, with the lowest values being obtained for particles in a vacuum or surrounded by nobel gas matrices and the highest values for a glass matrix. For gold nano-particle clusters in glass a value of 1.4 has been observed. It is also observed that A depends on the extent to which the metal particles are surrounded by the matrix, for example, if the particles are deposited on the surface of a substrate the value will be lower than if the particles are fully surrounded. The only data specifically for coated particles has been reported by Westcott *et al* [4], who used $A = 2$ to fit experimental data for gold coated silica nano-particles, attributing such a high value to internal grain boundaries created within the coating by the deposition process.

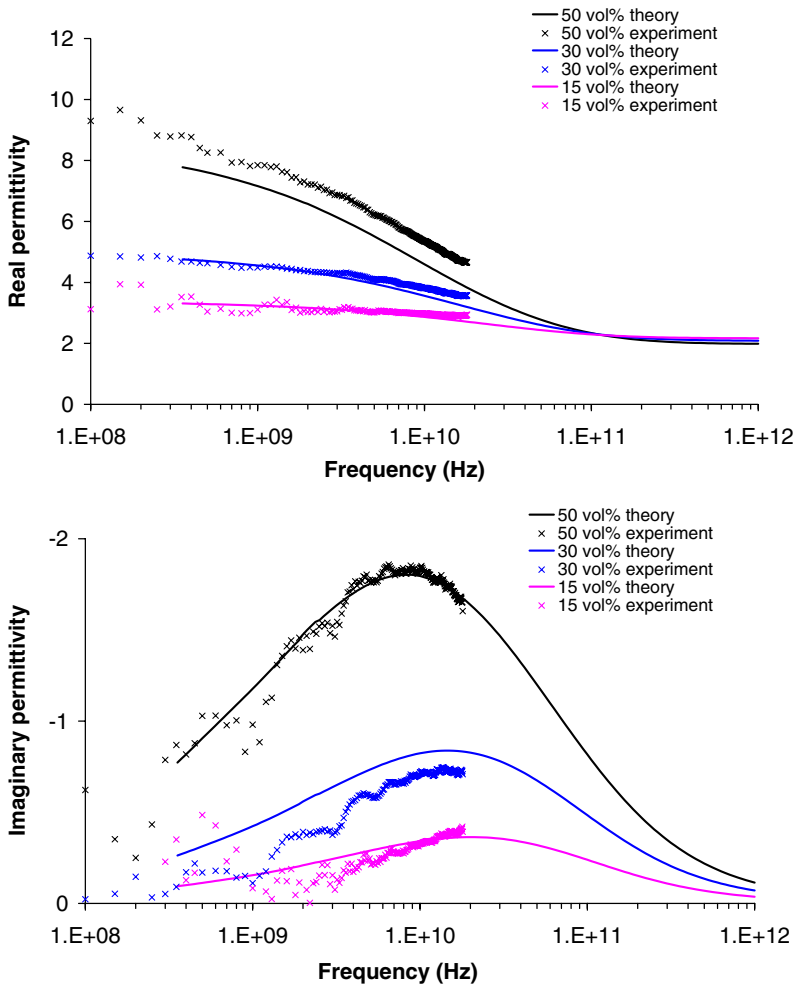

Figure 2. Comparison of the fit between theory and experiment for the dielectric absorption in a metal-coated particle filled composite assuming nano-scale surface scattering in the metal coating (using equations (6)–(8) as input to equation (1)) and a coating thickness distribution (mean thickness = 10 nm, standard deviation = 13 nm). Data is presented for filler concentrations 15, 30 and 50 vol%. The fit was achieved by setting the chemical interaction parameter A (from equation (7)) equal to 4500. Note: increasing magnitudes for traces correlate with increasing filler concentration.

that the tungsten coating is not continuous, since similar work on continuous gold nanoshells at optical frequencies does not observe a similarly large increase in electron scattering and concomitant downward shift in the relaxation frequency [4].

As a final point before presenting the new work, it is worth reviewing the closing observations of the previous work in relation to the quality of the fit between theory and experiment, as presented here in figure 2. Closer inspection of the figure reveals that the fit is best and 'good' at 50 vol%, especially when considering the loss peak, becoming 'acceptable' at 15 and 30 vol% filler concentrations. The particular concentration at which the fit is best (50 vol%) is not significant and is purely incidental because the fit parameters were optimized for this concentration. The critical observation is that the quality of the fit is not independent of filler concentration. This highlights that equation (1) provides too small a rate of change of the dielectric relaxation (absorption) frequency with filler concentration. There are a number of approaches that would increase this rate of change, such as including higher-order multipole interaction terms or implementing the renormalization method of Barrera *et al* [23] to account for interparticle correlation. But from a pragmatic perspective, an alternative view is that an intermediate position between the Sihvola–Lindell and Hanai–Bruggeman models is needed. The latter is based conceptually on the hypothesis that the presence of a particle size distribution acts to increase the rate of change of relaxation frequency with filler concentration. Nevertheless, it is important to note that none of these modifications to the model would provide further insight to the critical role of the metal coating or provide a means of further understanding or eliminating the chemical interaction parameter A from the model. Hence, the present work focuses more on the structure of the metal coating and the way in which it is modelled, being less concerned about the precise choice for the 'global' model of the filled composite (Sihvola–Lindell versus Hanai–Bruggeman).

2. Scanning electron microscopy of the filler particles

In the present work, the assumption regarding the uniformity and continuity of the metal coating has been tested through scanning electron microscopy (SEM). Secondary electron images were used to investigate the outermost alumina layer,

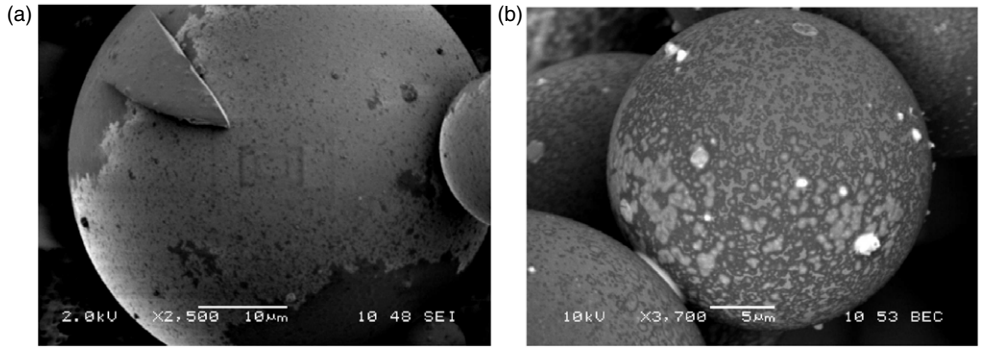

Figure 3. (*a*) Partial coating of alumina (lighter region) on a tungsten-coated glass microbubble. Surface debris is also visible. (*b*) Tungsten deposits (mid-grey patches) on a glass microbubble. The few lightest patches are surface debris.

revealing a continuous, but usually only partial, coating of the microbubbles. A typical image is shown in figure 3(*a*). Backscattering electron images were used to investigate the underlying tungsten layer, revealing a fairly uniform yet discontinuous morphology with island-like tungsten deposits, figure 3(*b*). The electron beam energy was also varied to aid interpretation.

A proper understanding of the interaction between the electron beam and the specimen is important for correct interpretation of the SEM micrographs. There are two categories of signals that result from collisions between primary incident electrons and the atoms of the sample. These are due either to elastic scattering or inelastic scattering. In an elastic scattering event, the direction of the incident electron is changed but its energy is conserved. Elastic scattering results from Rutherford scattering of the beam electrons with the nuclei of the sample atoms. Electrons that scatter in this way and later exit the sample are termed 'backscattering electrons'. They have high energy, equal to the accelerating potential of the microscope. In an inelastic scattering event, energy is transferred from incident electrons to the target material, resulting in a decrease in kinetic energy of the incident electrons. Interaction of the beam electrons with the target atoms can eject the loosely bound electrons of the conduction band. These ejected electrons are termed 'secondary electrons'. These usually have an initial kinetic energy of between 0 and 50 eV.

The depth of the electron interaction area depends on the atomic number of the specimen and the energy of the incoming beam electrons. The Kanaya–Okayama range equation can be used to obtain an approximate depth dimension of the electron interaction area [24]. At 0° tilt,

$$R_{\mathrm{KO}} = \frac{0.027\alpha E_0^{1.67}}{Z^{0.889}\rho}. \tag{9}$$

In equation (9), R_{KO} is the depth in micrometre, α is the average atomic weight of the target material in grams per mole, E_0 is the electron energy in kiloelectronvolt, Z is the atomic number of the target and ρ is the density in grams per centimetre cube. From this equation it can be seen that penetration into the target is lower for high-atomic number material than for low-atomic number material, due to higher probability of elastic scattering. Backscattered electrons are, therefore, generated at various depths below the target surface, depending upon the atomic number of the target material. On the other hand, secondary electrons tend to emerge from a fairly constant, shallow, sampling depth due to their low kinetic energy. The depth at which information is obtained by secondary electrons is about 1/100 of that of backscatter electrons, whereas the information depth yielded by backscatter electrons is approximately 0.3 times that of the Kanaya–Okayama range. For tungsten, $R_{\mathrm{KO}} = 145$ nm, calculated with parameters $\alpha = 183.84$ amu, $E_0 = 7$ keV, $Z = 74$ and $\rho = 19.25\,\mathrm{g\,cm^{-3}}$. The calculated depth from which information is obtained from backscatter electrons is therefore approximately 43 nm. This value is somewhat greater than the nominal thickness of the tungsten coating, but in general equation (9) is considered more accurate for depths measurable in microns.

In this study, tungsten-coated glass microbubble powders were examined. The thickness of the tungsten layer was nominally 20 nm, and the tungsten coating had an aluminium oxide layer of thickness approximately 3 nm as an exterior coating. The mean radius of the glass microbubbles was around 15 μm. Of primary interest was investigation of the level of homogeneity of the tungsten layer. Since the outer aluminium oxide layer prevented direct observation of the tungsten layer, different accelerating voltages and signal detector configurations were used in the investigation. By varying the accelerating voltage, the depth of penetration was varied, with the effect that the detected backscattered signal originated from different depths within the sample. This allowed the tungsten layer to be observed through the outer aluminium oxide layer. Samples were coated with carbon prior to SEM examination, to provide a conducting pathway by which the electrons could disperse. This prevents charging of the insulating aluminium oxide and consequent blurring of the images.

Firstly, the exterior coating of aluminium oxide was examined. A low accelerating voltage and secondary electrons were used for image formation, to limit beam penetration through the aluminium oxide layer and ensure that the image obtained was generated from electrons exiting the top region of the interaction area. It was observed that the majority of the particles did not have a complete aluminium oxide coating, but the coating did cover a large area on the surface of the particles. This was true for eight out of eleven particles examined. Three appeared to be fully coated although only one side of the sphere was visible for each examination. A typical micrograph is shown in figure 3(*a*).

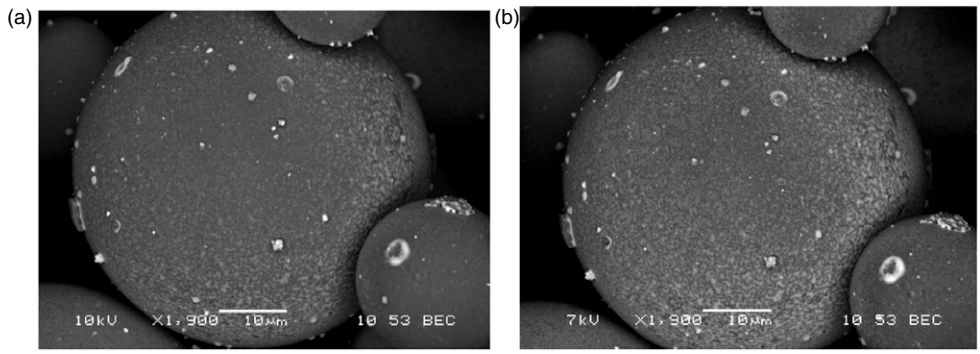

Figure 4. Backscattering electron micrographs (*a*) 10 keV accelerating voltage, (*b*) 7 keV accelerating voltage gives a slightly sharper image, especially on the top (centre) of the spherical particle.

Secondly, the tungsten layer was examined. Since this layer was for the most part obscured by the aluminium oxide layer, a higher accelerating voltage was used (10 keV), and the backscattered signal was used for image formation. A typical image is shown in figure 3(*b*). All ten particles examined exhibited similar features. It should be noted that, in an image created by backscattering electrons (BSE), as atomic number increases not only does beam penetration decrease, as stated previously, but the probability of backscattering also increases. Thus, the tungsten layer can be seen as pale regions (in which there is a greater density of backscattered electrons) in the micrographs obtained in this way. Note that the islands of tungsten in figure 3(*b*) can be seen more clearly towards the particle sides than on top (centre). The reason for this is believed to be that 10 keV was slightly higher energy than optimum for observing the depth of interest for these particles; nominally less than 23 nm. Viewing the sides of the spherical particles creates an effect of tilting, and thus the radial depth of penetration into the particle is reduced. In this case, a greater proportion of the signal from the sides of a particle is generated within the tungsten layer, giving a higher signal-to-noise ratio and a sharper image. This hypothesis is supported by micrographs shown in figures 4(*a*) and (*b*). These two BSE micrographs of the same particle were obtained using accelerating voltages of 10 keV and 7 keV, respectively. The pale regions of tungsten on the top (centre) of the spheres are clearer in the image obtained using 7 keV accelerating voltage.

In summary, the aluminium oxide layer was seen to cover the majority of the surface of a typical particle, but some areas were not coated at all. The tungsten layer was homogenous but not continuous, consisting of a fairly uniform distribution of small islands. The average dimension of a typical tungsten island is approximately 1 μm.

3. Image analysis

Image analysis was performed in an attempt to quantify the proportion of the particle surface covered by tungsten. Four regions were selected from BSE micrographs of different particles (figure 5).

The areas chosen were free from surface debris and were selected from the central region of a particle image, to reduce curvature effects. Curvature was not corrected for explicitly. These images were converted to 8-bit grey-scale format to assist with selecting the threshold at which a pixel was identified as being tungsten, or not. The area percentage of each phase was then determined. Results are presented in table 2.

4. Non-continuous coatings—a role for a percolation-based sub-model

It is clear from the scanning electron micrographs that the tungsten coating is far from continuous, potentially supporting the use of an extremely large value for the chemical interaction parameter, as in the previous work, but also providing a substantial imperative to develop an improved sub-model for the permittivity of the tungsten layer. The images obtained demonstrate immediate similarities to percolation networks, and to cermet films in particular [25]. Hence, the application of a percolation-based effective medium model to determine the permittivity of the tungsten layer is the obvious next extension to the work. But before this is done it is beneficial to review relevant literature. Indeed, Westcott and Halas [26] have recently demonstrated the distinct difference between continuous and semicontinuous metal films on nano-particle surfaces in terms of their optical properties and electron dynamics. In fact, the boundary between semicontinuous and continuous films is defined as the percolation threshold.

The earlier work on cermet films, as summarized by Coutts [25], provides useful insight into the likely conduction mechanisms operating in the coated particles studied here. The resistance of cermet films (a thin film mixture of conducting and insulating phases) can vary significantly (by orders of magnitude) from sample to sample, even when preparation conditions are held constant. This is typical of a percolation-driven phase (conductor–insulator) transition for samples near the transition point, since they become sensitive to small fluctuations in conditions, and increasingly so when the properties of the constituents are in strong contrast as is the case for a good metal mixed with a good insulator. A further observation is that the temperature coefficient of resistance of these mixed materials can take both positive and negative values. This is more deeply instructive as it indicates the presence of more than one conduction mechanism within the coating.

The microstructure of mixed material coatings can adopt different classes of microstructure depending on the relative proportions of the constituents. At low concentrations of conductor, the conductor is likely to exist as small isolated islands. As the concentration increases, more islands exist,

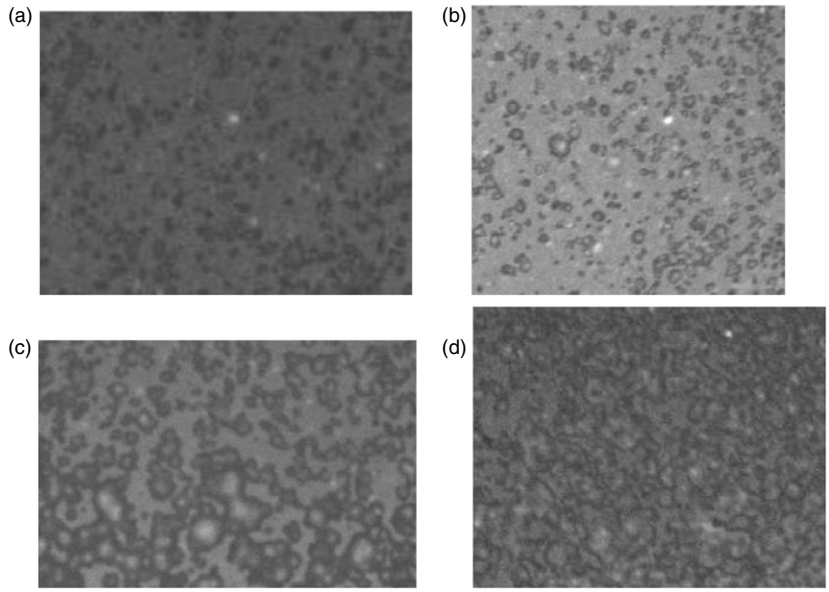

Figure 5. BSE micrographs obtained using 10 keV accelerating voltage for a selected central region of four different particles.

Table 2. Area percentage of tungsten obtained from analysis of four images, (*a*)–(*d*), shown in figure 5.

Image	Area % tungsten
(*a*)	73
(*b*)	81
(*c*)	45
(*d*)	57
Mean ± standard deviation	64 ± 8

and the mean island size tends to grow. Isolated islands can become connected, but the degree of connection can vary from full overlap to connection by very thin 'capillary' channels, where the channel width is much thinner than the island size. Eventually, extended networks of connected islands will form and, at a certain concentration, a network will exist that spans the sample. Initially, conduction across this 'global' network is likely to be dominated by the resistance of the narrow channels but, as further conductor is added, the number of narrow channels will diminish until the point where a continuous coating exists. However, this progression through discontinuous, then semi-continuous to continuous coating structure is not likely to occur in discrete stages, and it is highly likely that, at intermediate conductor concentrations, each of the structure types is present in different regions of the coating. Such an evolutionary process for coating formation underpins the expectation for multiple conduction mechanisms existing simultaneously.

The two principle types of conduction that may be observed are 'normal' metallic conduction, through the capillaries, and activated conduction between conducting islands. Clearly, it is when the conductivity derived from each mechanism is similar in magnitude that both mechanisms should be included in any model. It is stated by Coutts that, whilst both mechanisms are required to account for the temperature dependence of the resistance, the resistance itself is dominated by metallic conduction through the capillaries. It is now perhaps obvious that it is the broad distribution of capillary widths that can create a broad distribution in the degree of electron scattering. Hence, in relation to the modelling approach of the previous work [9], it is now apparent that it may not be the coating thickness and thickness distribution that needs to be modelled but, rather, the size and distribution of conducting capillaries.

In the present work it is the macroscopically averaged response—the bulk permittivity of the coating—that is required, and it is questioned whether it is necessary to delve too deeply into the microscopic (or indeed nanoscopic) reality of the coating structure. If it is assumed that the distribution of conducting material (islands) over the particle surface is truly random then the transition from a discontinuous to a continuous film should be accounted for by a percolation theory-based model. Moreover, the properties of semicontinuous films would naturally fall into the power law scaling region of the percolation theory; the region at and near the percolation threshold. Fortunately, such a percolation-based model for conductivity, and hence permittivity, exists in the form of the McLachlan general effective medium model [27] as defined by equation (10) using subscripts for the permittivity terms that are relevant to the current work (ε_1 is the permittivity of the tungsten coating and is the parameter to be determined, $\varepsilon_{\text{alumina}}$ is the permittivity of the aluminium oxide outer coating, taken as representative of the insulating phase in the semi-continuous coating and $\varepsilon_{\text{tungsten}}$ is the permittivity of the tungsten component given by equations (6)–(8)). The additional parameters are the fraction of tungsten in the semi-continuous coating, f_{tungsten}, the fraction of the conducting phase at which percolation occurs (referred to as the percolation threshold), f_c, and the power law exponents, s and t.

$$(1 - f_{\text{tungsten}}) \left[\frac{\varepsilon_{\text{alumina}}^{1/s} - \varepsilon_1^{1/s}}{\varepsilon_{\text{alumina}}^{1/s} + ((1 - f_c)/f_c)\varepsilon_1^{1/s}} \right] + f_{\text{tungsten}} \left[\frac{\varepsilon_{\text{tungsten}}^{1/t} - \varepsilon_1^{1/t}}{\varepsilon_{\text{tungsten}}^{1/t} + ((1 - f_c)/f_c)\varepsilon_1^{1/t}} \right] = 0. \qquad (10)$$

Equation (10), in the form presented here, is usually applied to three-dimensional (3D) percolation networks, in which case f_{tungsten} is the volume fraction of tungsten in the composite material. However, it is not obvious whether these tungsten coatings should be treated as two-dimensional (2D) or 3D networks. Making this judgement is critical since, theoretically for truly random networks, the percolation power law exponents s and t adopt values which are purely a function of the dimensionality of the network [28]. The percolation threshold also depends on the type of filling geometry that is assumed, which in turn is related to the dimensionality of the network and the shape of the filler 'particles'. Of course these parameters may alternatively be derived experimentally. Again, evidence from the literature is taken to support the decision regarding the likely dimensionality of the coating. Lebovka *et al* have modelled the deposition of thin films where either only conducting particles are deposited or they are co-deposited with insulating particles using ballistic, random and mixed deposition rules [29]. The coatings under investigation here correspond to the case where only conducting particles are deposited. In this case, Lebovka *et al* have shown that both sets of deposition rules lead to 2D networks although there is a difference in the number of monolayers required to achieve percolation, ranging from 0.89832 for ballistic and 2.605 for random deposition. In contrast, co-deposited coatings show a transition from 2D to 3D network response as the coating thickness increases. By way of experimental evidence, Arnason *et al* have reported resistance measurements as a function of film thickness for thin thermally evaporated silver coatings [30]. A percolation transition was observed as the film thickness increased, with the resistance exhibiting a power-law dependence as a function of film thickness relative to a critical 'transition' thickness. The power law exponent matches the theoretical value of 1.299 for 2D percolation. The transition thickness was 19.2 nm, and the power law response was observed for thicknesses in the range 19.2–40 nm, which is similar to the thickness of the tungsten coatings studied here, as stated by the manufacturer. Further evidence of a percolation transition at film thicknesses of approximately 40 nm for a range of metals is provided by Antonets *et al* [31] and Tanikawa *et al* [32]. Hence, we assume with some confidence, that the tungsten coatings studied here will behave as a 2D percolation network. However, the percolation transition may occur at an arbitrary tungsten area fraction, which may be estimated from the image analysis presented in section 3.

5. Parametric trends in dielectric response

Before assessing the ability of a revised model, in which the conductive coating is modelled as a 2D percolating network, to fit the experimental data, it is instructive to investigate the influence of the percolation model parameters on the effective dielectric response of a composite filled with such metal-coated particles. The influence of the model parameters on the dielectric response of the composite medium is presented in terms of three characteristics of the loss peak observed in the calculated imaginary permittivity. The characteristics selected are (i) the maximum value of the imaginary permittivity (the relaxation amplitude), (ii) the relaxation frequency (the frequency at which the imaginary permittivity is maximum) and (iii) the relative full-width-half-maximum (FWHM) bandwidth of the peak (i.e. the FWHM bandwidth normalized to the relaxation frequency). For clarity, these calculations were performed assuming no distribution of tungsten coating thickness; hence this parameter takes the mean value of 20 nm (see table 1) unless otherwise stated. The default values of all model parameters used in this analysis are summarized in table 3, noting that, unless otherwise stated, the area fraction of tungsten forming the coating is at the percolation threshold. The analysis presented in the following subsections demonstrates the complex and subtle nature of the dependence of the dielectric response on the model parameters.

Table 3. Default values of model parameters used in the parametric analysis presented in section 5.

Parameter	Default value
Filler volume fraction	0.3
Tungsten area fraction	0.5
Coating percolation threshold (critical area fraction)	0.5
Percolation exponent s	1.299
Percolation exponent t	1.299
Tungsten coating thickness (nm)	20
Core particle radius (μm)	15
Coating quality factor A	10
Permittivity of medium filling 'holes' in tungsten coating	8.79 (Alumina)

5.1. Dependence on filler concentration

Figure 6 presents the calculated dependence of the loss peak characteristics as a function of increasing filler volume fraction. It is highlighted that there is a strong dependence of the relaxation frequency (decreasing) and relaxation amplitude (increasing) with increasing filler particle concentration. The relative peak bandwidth increases slowly with increasing filler concentration.

5.2. Dependence on tungsten area fraction

Figure 7 presents the calculated dependence of the loss peak characteristics as a function of increasing tungsten area fraction. The tungsten area fraction is shown relative to the coating percolation threshold, as defined by equation (11). Hence, negative values for the normalized tungsten fraction represent actual tungsten fractions below the percolation threshold. Positive values for the normalized tungsten fraction represent actual tungsten fractions above the percolation threshold. The normalized tungsten fraction is zero when the actual tungsten fraction is at the percolation threshold:

$$f_{\text{normalized}} = \frac{f_{\text{tungsten}} - f_{\text{c}}}{f_{\text{c}}}. \tag{11}$$

It is observed that the relaxation frequency is at a minimum at the coating percolation threshold, whilst relative bandwidth is at a maximum. This implies that achieving the lowest relaxation frequencies and the broadest relaxation peaks is critically related to the occurrence of an insulator–conductor transition in the coating. Such a trend is not predicted by the previous model [9] for a thin, continuous tungsten coating. The relaxation amplitude is seen to increase with increasing tungsten area fraction.

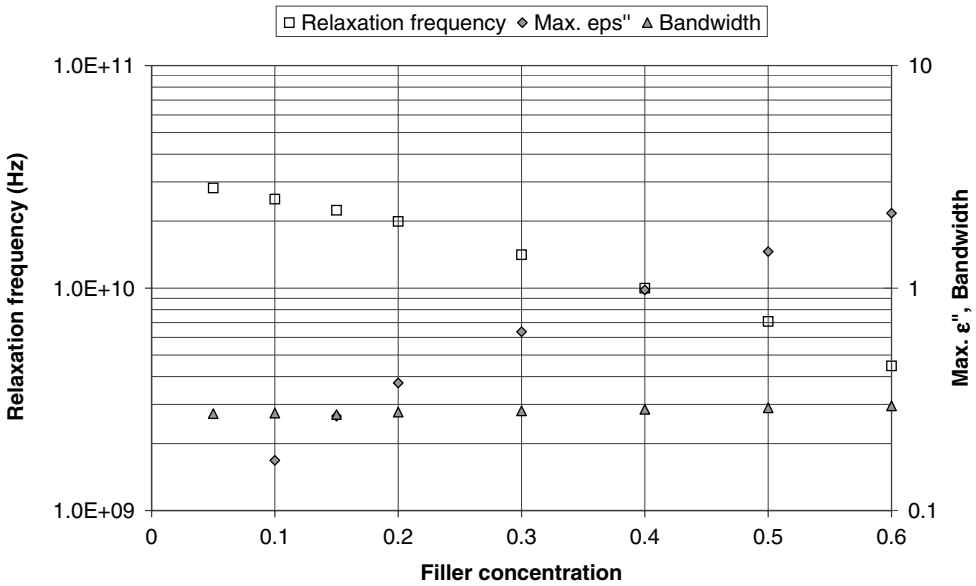

Figure 6. Calculated dependence of loss peak characteristics as a function of filler particle concentration.

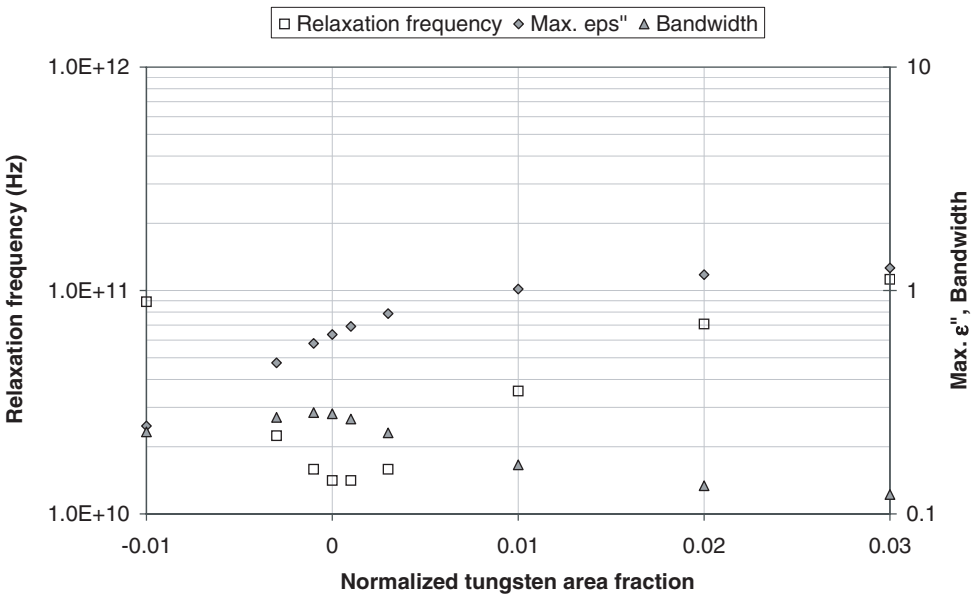

Figure 7. Calculated dependence of loss peak characteristics as a function of tungsten area fraction.

5.3. Dependence on tungsten coating thickness when the coating is at the percolation threshold

Figure 8 presents the calculated dependence of the loss peak characteristics as a function of increasing coating thickness, relative to the core particle radius, for a coating that is at the percolation threshold. It is seen that the relaxation frequency increases rapidly with increasing coating thickness. Whilst a relative coating thickness is used to produce the figure, it is considered more likely that the regimes of dependence for the other characteristics are in fact related to the actual coating thickness. This reasoning is consistent with there being decreasing significance of surface scattering of conduction electrons as the coating thickness increases beyond the nanometric region ($\geqslant$100 nm). The relaxation amplitude remains approximately constant for nanometric coating thicknesses ($<$100 nm), but increases for thicker coatings. Similarly, the relative peak bandwidth decreases slowly with increasing coating thickness in the nano-metric region, with a more rapid decrease for thicker coatings.

5.4. Dependence on percolation exponent t

Figure 9 presents the calculated dependence of the loss peak characteristics with increasing value of the percolation threshold t. This exponent relates to the power-law response of the coating conductivity, in this case. A value of $t = 1$ (with $s = 1$) would correspond to representing the effective dielectric properties of the coating with the symmetric Bruggeman effective medium model [33]; it has already been stated that the universal value for 2D percolation networks is 1.299; for 3D percolation networks the universal value is 1.9;

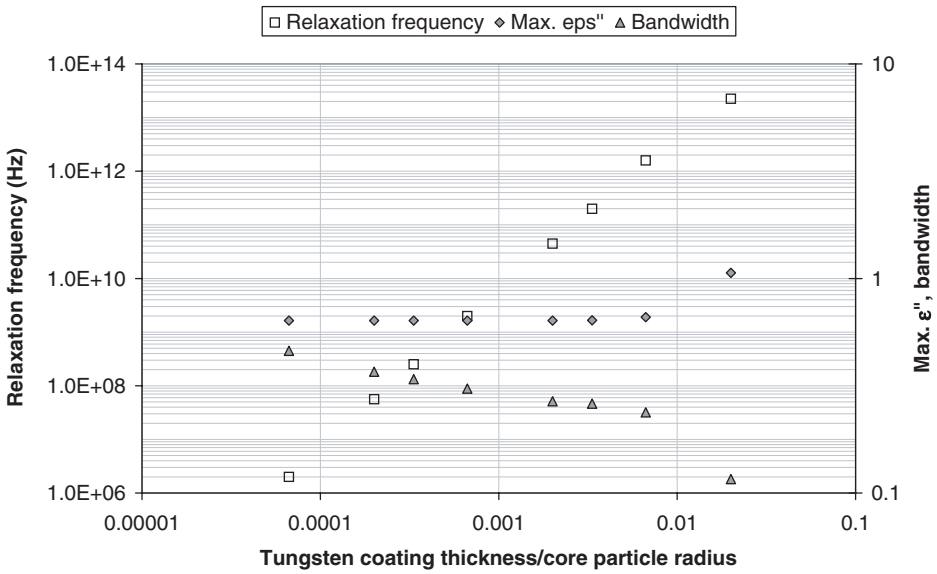

Figure 8. Calculated dependence of loss peak characteristics as a function of tungsten coating thickness when the coating is at the percolation threshold.

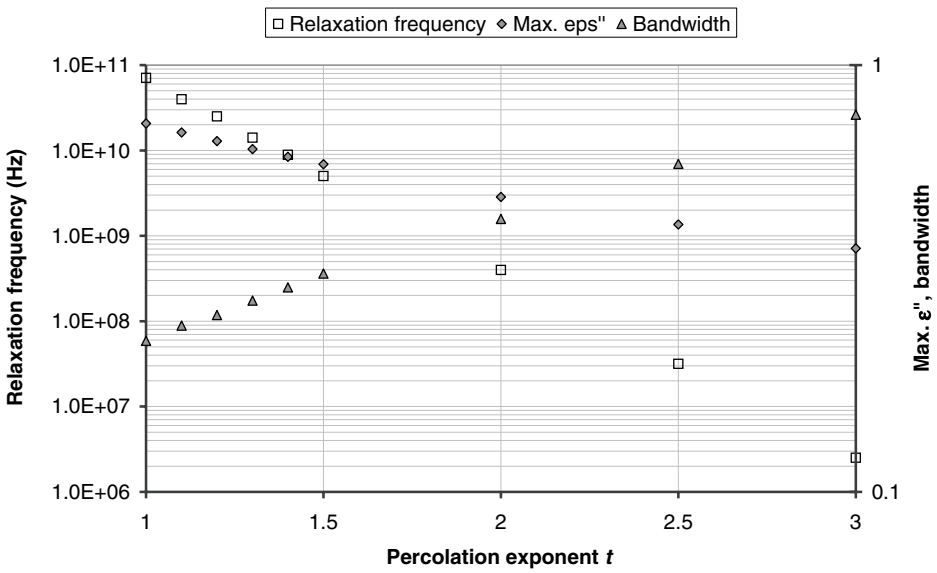

Figure 9. Calculated dependence of loss peak characteristics as a function of percolation exponent t.

moreover, larger values have been reported experimentally for a number of years and, from a theoretical perspective, are attributed to non-perfect randomness and the influence of inter-particle contact and charge tunnelling on conduction [34]. This parameter has a strong influence on all three loss peak characteristics. The relaxation frequency and relaxation amplitude both decrease with increasing exponent value. The relative peak bandwidth increases with increasing exponent value. Trends with the exponent s are not included here, since s is more relevant to the description of discontinuous coatings below the percolation threshold.

5.5. Dependence on tungsten coating chemical interaction (quality) factor A

Figure 10 presents the calculated dependence of the loss peak characteristics with increasing value of the coating chemical interaction (quality) factor, A. This parameter has a strong influence on the relaxation frequency, with the relaxation frequency decreasing as A increases, but only weakly influences the relaxation amplitude and relative peak bandwidth. The relaxation amplitude is almost independent of A.

5.6. Dependence on the permittivity of the insulating medium filling the 'holes' in the semi-continuous tungsten coating

Figure 11 presents the calculated dependence of the loss peak characteristics with increasing permittivity of the insulating medium filling the 'holes' in the semi-continuous tungsten coating. In relation to the experimental system studied herein, it is difficult to determine exactly what medium (if any) fills the 'holes' in the semi-continuous tungsten coating and, therefore,

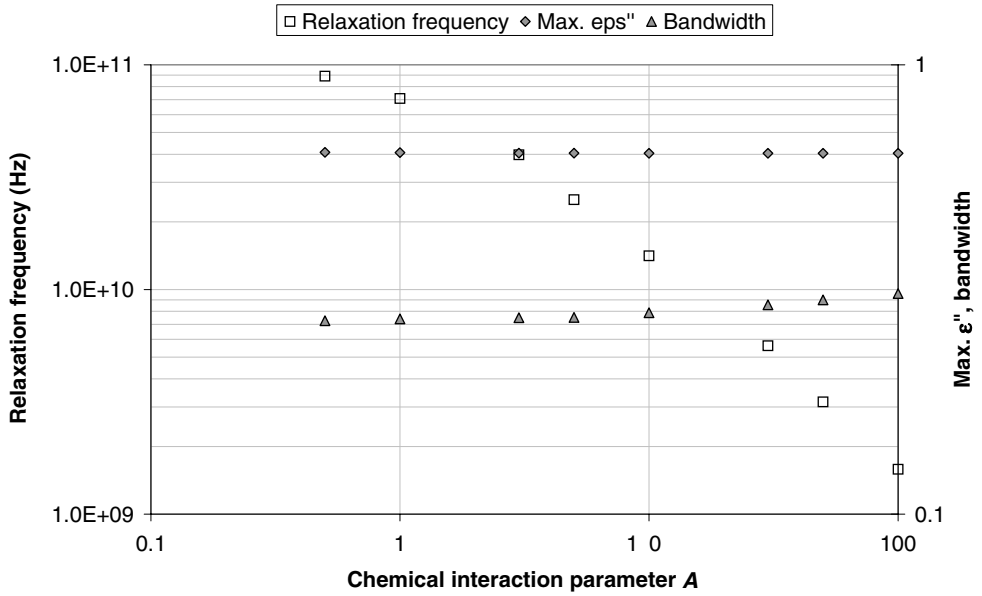

Figure 10. Calculated dependence of loss peak characteristics as a function of coating chemical interaction (quality) factor *A*.

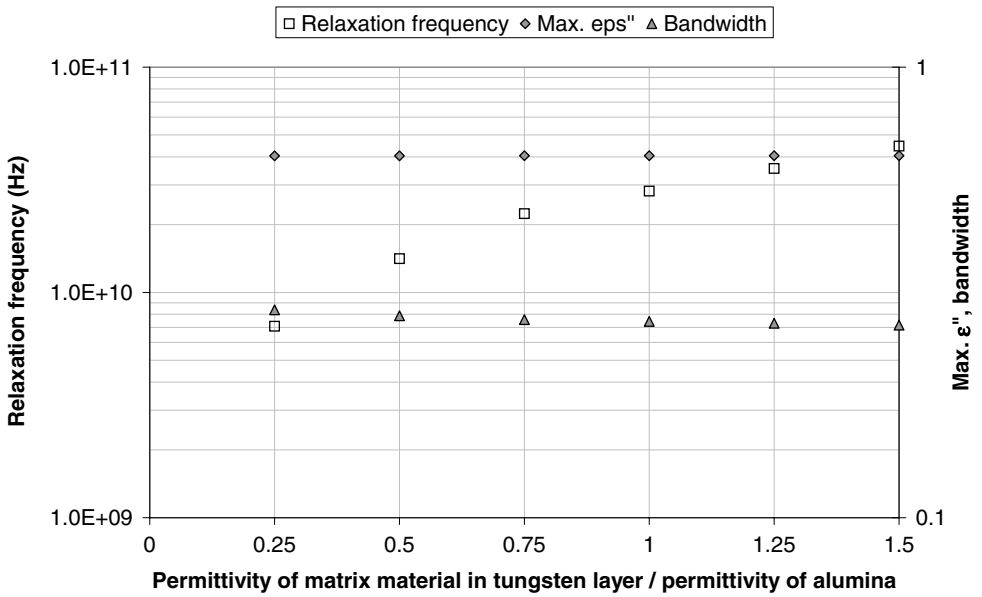

Figure 11. Calculated dependence of loss peak characteristics as a function of permittivity of the insulating medium filling the 'holes' in the semi-continuous tungsten coating.

it is difficult to assign an appropriate value of permittivity for this medium. The medium may be alumina, but the micrograph presented in figure 3(*a*) highlights that the alumina coating is only partial. Furthermore, the alumina coating is thinner than the tungsten coating. Hence, both the permittivity of the silica core shell and that of the surrounding host medium (wax) may contribute to the background dielectric environment of the tungsten. Therefore, the permittivity of the 'hole' filling (i.e. that of the coating matrix medium) is shown in the figure as a quantity that is relative to the permittivity of alumina. The figure shows that the relaxation frequency increases significantly with increasing coating matrix permittivity, whilst the relative bandwidth decreases very slowly. Again, the relaxation amplitude is almost independent of this parameter. In terms of fitting the experimental data (see section 6), this parameter may be legitimately taken as a free variable in the range of approximately 0.1 (for air) to 1, since of all the options alumina has the largest permittivity.

6. Comparison with experiment

The parametric analysis has demonstrated the complex dependence of the total dielectric response on the parameters of the percolation model for the coating. It therefore remains to demonstrate the validity of this model by comparison with experimental data presented previously [9]. In the first instance, figure 12 shows that an improved fit, compared with that achieved using the earlier model (see figure 2), is achievable without the introduction of any distribution

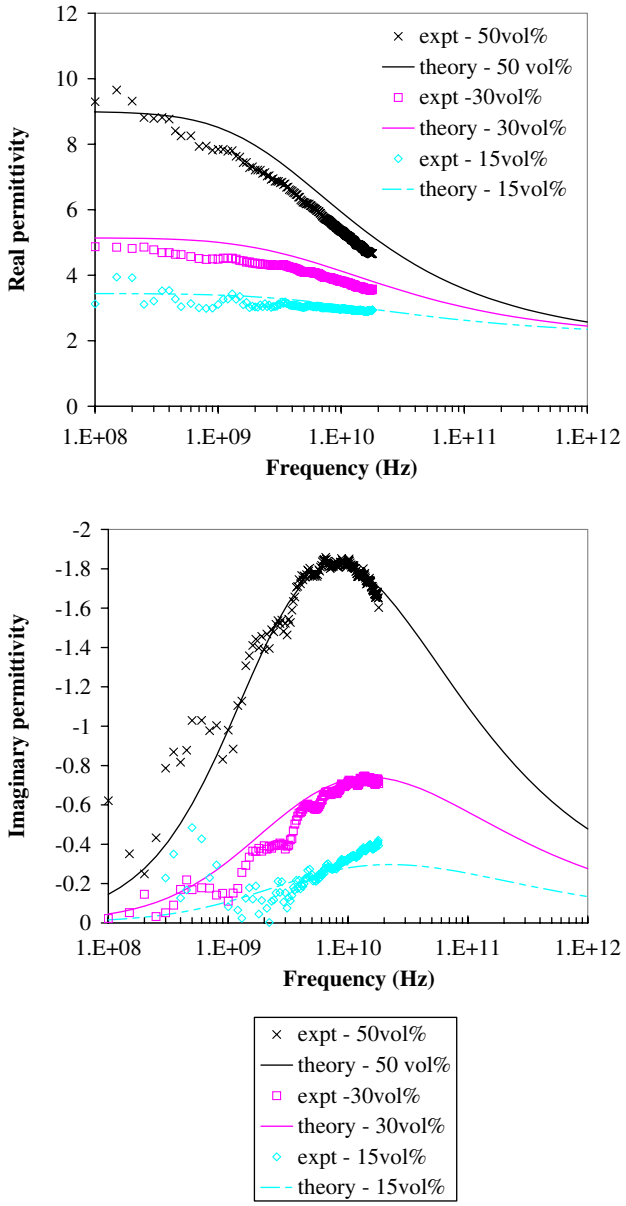

Figure 12. Comparison of percolation-based model to experimental data for the complex permittivity of composites formed from tungsten coated microspheres dispersed in paraffin wax (fixed coating area fraction and thickness).

of coating thickness or indeed of coating area fraction or indeed an anomalous value for the coating quality parameter A. Moreover, the majority of the model parameters take reasonable values when compared with the best available supporting evidence (see comparison in table 4). Yet it is significant that the fit requires an adjusted percolation threshold that is below, but very close to, the coating area fraction and a non-universal (slightly larger) value for the percolation power law exponent t. Forcing the value of the tungsten area fraction to be very close to the percolation threshold in the fit is a concern because the range of area fractions observed from the image analysis is broad and probably spans the percolation threshold. In other words, the experimental system would appear to achieve the measured dielectric response without requiring such closeness between these parameters. Hence,

Table 4. Fit parameters used for figure 12 compared to best supporting information for parameter values.

Parameter	Value used in fit	Value suggested by supporting evidence
Tungsten area fraction	0.64	0.64 ± 0.08
Coating percolation threshold (critical area fraction)	0.636816	0.5
Percolation exponent s	1.299	1.299
Percolation exponent t	1.9	1.299
Tungsten coating thickness (nm)	20	20
Core particle radius (μm)	15	15
Coating quality factor A	1	1
Permittivity of medium filling 'holes' in tungsten coating	4.4	8.79 (Alumina)

the fit is not as satisfactory as first assumed, because the experimental results are apparently not so sensitive to closeness of the coating area fraction to the percolation threshold.

To counter this deficiency of the percolation model, a normal distribution of coating area fraction (for a fixed coating thickness) is introduced following the approach used earlier for the coating thickness distribution [9]. The revised fit is presented in figure 13 and uses the fit parameters given in table 5. The resulting fit is again good. In this case, the coating percolation threshold and mean coating area fraction are set at the expected values, although it is noted that the distribution in coating area fraction is not as wide as suggested by the image analysis, and the percolation exponent t has been increased although not necessarily to an unrealistic value. However, caution should be placed in accepting these fit parameters with a high degree of confidence, since the expected values provided by the supporting evidence and theories have not been extensively substantiated in the current study. For example, only a small number of coatings have been analysed, and the threshold setting for the image analysis is somewhat arbitrary and subjective. Furthermore, to make a more realistic model of the coating would require consideration of how the distribution of coating area fractions amongst the ensemble of coated particles is related to the coating thickness. This would require making some major assumptions regarding the coating deposition and growth process employed in the fabrication of the particles used in this study and/or further detailed experimental investigation of the same process. In addition, it would be relevant to determine the most appropriate coating percolation threshold, perhaps by analogy to the modelling work of Lebovka *et al* [29], which adopts a pseudo 3D structure for coatings even though they exhibit power-law exponents, which are indicative of 2D percolation. The current work has used a percolation threshold of 0.5, which is valid for a purely planar square lattice and which represents a very coarse assumption when viewed in the context of the images presented in figure 5. Nevertheless, the analysis presented herein provides strong support for the use of a percolation-based model to describe the coating. Moreover, the percolation-based model should prove more reliable than the previous model [9] in providing design guidelines for engineering the radio and microwave dielectric properties of composites filled with semi-continuous, metal-coated particles.

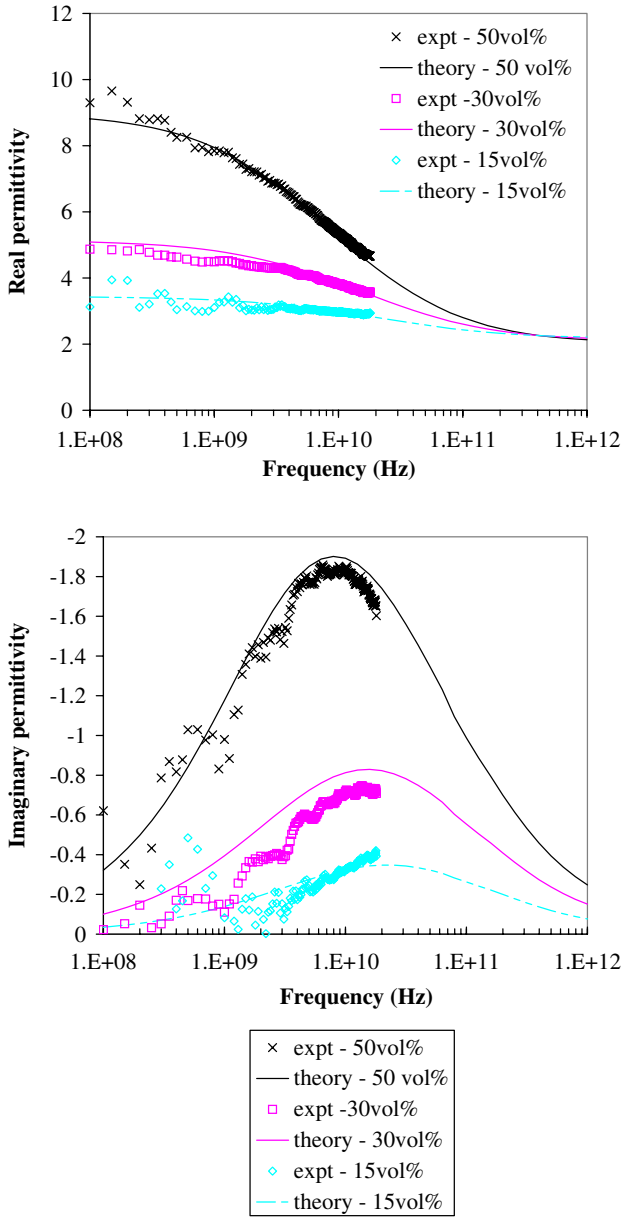

Figure 13. Comparison of percolation-based model to experimental data for the complex permittivity of composites formed from tungsten coated microspheres dispersed in paraffin wax (with a distribution of coating area fraction and fixed coating thickness).

7. Conclusions

A percolation-based model (using McLachlan's general effective medium equation) to represent the complex permittivity of a semi-continuous metal coating has been introduced to a model to determine the effective permittivity of a composite filled with particles with such coatings. The coated particle geometry can be used to engineer dielectric absorption in composites for low frequency (radio and microwave) applications when the coating thickness is in the nanometre range. Parametric analysis highlights the complex dependence and sensitivity of absorption peak characteristics (relaxation frequency, broadening and strength) on the percolation parameters of the metal coating. Moreover, it has been shown that the percolation-based model can provide an improved fit to available experimental data using less extreme values of fit parameters, compared with a previously developed model that assumed the metal coating to be thin but continuous [9]. Theory and experimental evidence, including SEM analysis presented herein, support the fit parameters obtained. It is demonstrated that a coating with conductive component very near the percolation threshold can provide a good fit to the experimental data. In practice, achieving coatings that are very close and, specifically, close to the percolation threshold may be difficult to engineer. However, it is shown that a more realistic fit can also be achieved when a distribution of coating area coverage is added, utilizing an ensemble of particles with coating area fractions distributed about the percolation threshold. Hence, design guidelines, which are related to the coating topology, can now be developed with greater confidence.

Table 5. Fit parameters used for figure 13 compared to best supporting information for parameter values.

Parameter	Value used in fit	Value suggested by supporting evidence
Tungsten area fraction (mean ± standard deviation)	0.64 ± 0.035	0.64 ± 0.08
Coating percolation threshold (critical area fraction)	0.5	0.5
Percolation exponent s	1.299	1.299
Percolation exponent t	6.4	1.299
Tungsten coating thickness (nm)	20	20
Core particle radius (μm)	15	15
Coating quality factor A	1	1
Permittivity of medium filling 'holes' in tungsten coating	4.4	8.79 (Alumina)

Acknowledgments

The authors most gratefully acknowledge the supply of particles and related technical information by Dr Craig Chamberlain of 3M, St Paul, MN, USA. I Youngs' work was funded by the Ministry of Defence. N Bowler's work was performed at the Center for NDE at Iowa State University with funding from the Air Force Research Laboratory through S&K Technologies, Inc. on delivery order number 5007-IOWA-001 of the prime contract F09650-00-D-0018.

References

[1] Neeves A E and Birnboim MH 1989 *J. Opt. Soc. Am.* B **6** 787–96
[2] Haus J W, Zhou H S, Takami S, Hirasawa M, Honma I and Komiyama H 1993 *J. Appl. Phys.* **73** 1043–8
[3] Oldenburg S J, Averitt R D, Westcott S L and Halas N J 1998 *Chem. Phys. Lett.* **288** 243–7
[4] Westcott S L, Jackson J B, Radloff C and Halas N J 2002 *Phys. Rev.* B **66** 155431-1-5
[5] Gindrup W L 1986 *US Patent* No 4,624,798
[6] Janos W A 1994 *US Patent* No 5,298,903
[7] Kim S-S, Kim S-T, Ahn J-M and Kim K-H 2004 *J. Magn. Magn. Mater.* **271** 39–45

[8] Chamberlain C S, Brennan J V, Gettinger C L and Wilson R W 2003 *US Patent* No 6,562,448
[9] Youngs I J, Bowler N, Lymer K P and Hussain S 2005 *J. Phys. D: Appl. Phys.* **38** 188–201
[10] Chamberlain C S, Connell G and Tait W C 1995 *US Patent* No 5,389,434
[11] Chamberlain C S private communication
[12] *3M Microspheres Selection Guide* January 2003
[13] Potter Industries Inc. *Materials Safety Data Sheet for Spheriglass ® Glass Spheres E-Glass* 26 February 2005
[14] von Hippel A R 1954 *Dielectric Materials and Applications* (New York: Wiley)
[15] Weast R 1977 *CRC Handbook of Chemistry and Physics* (Baton Rouge, FL: CRC Press)
[16] Nnolim N, Tyson T and Axe L 2003 *J. Appl. Phys.* **93** 4543–60
[17] Chakraborty B, Pickett W and Allen P 1976 *Phys. Rev.* B **14** 3227–30
[18] Sihvola A H and Lindell I V 1992 Polarizability modelling of heterogeneous media *Dielectric Properties of Heterogeneous Materials* ed A Priou (New York: Elsevier) chapter 3, pp 101–51
[19] Hovel H, Fritz S, Hilger A, Kreibig U and Vollmer M 1993 *Phys. Rev.* B **48** 18178–88
[20] Granqvist C G and Hunderi O 1978 *Z. Phys.* B **30** 47–51
[21] Barrera R G, Villaseñor-Gonzàlez P, Mochán W L and Monsivais G 1990 *Phys. Rev.* B **41** 7370–6
[22] Oshchepkov S L and Sinyuk A F 1998 *J. Colloid Interface Sci.* **208** 137–46
[23] Barrera R G, Monsivais G and Mochan W L 1988 *Phys. Rev.* B **38** 5371–9
[24] Goldstein J I, Newbury D E, Echlin P, Joy D C, Fiori C and Lifshin E 1981 *Scanning Electron Microscopy and X-ray Microanalysis* (New York: Plenum) pp 72–4
[25] Coutts T J 1974 *Electrical Conduction in Thin Metal Films* (Amsterdam: Elsevier) pp 224–36
[26] Westcott S L and Halas N J 2002 *Chem. Phys. Lett.* **356** 207–13
[27] McLachlan D S and Heaney M B 1999 *Phys. Rev.* B **60** 12746–51
[28] Stauffer D and Aharony A 1994 *Introduction to Percolation Theory* (London: Taylor and Francis)
[29] Lebovka N I, Manna S S, Tarafadr S and Teslenko N 2002 *Phys. Rev.* E **66** 066134
[30] Arnason S B, Herschfield S P and Hebard A F 1998 *Phys. Rev. Lett.* **81** 3936–9
[31] Antonets I V, Kotov L N, Nekipelov S V and Golubev Y A 2004 *Tech. Phys.* **49** 24–7
[32] Tanikawa T, Matsuda I, Nagao T and Hasegawa S 2001 *Surf. Sci.* **493** 389–98
[33] Bruggeman D 1935 *Ann. Phys. (Leipzig)* **24** 636–64
[34] Youngs I J 2002 *J. Phys. D: Appl. Phys.* **35** 3127–37